# *Ab initio* molecular dynamics study of the metallization of liquid selenium under pressure

Satoshi Ohmura and Fuyuki Shimojo
*Department of Physics, Kumamoto University, Kumamoto 860-8555, Japan*
(Received 13 January 2011; revised manuscript received 6 March 2011; published 21 April 2011)

The microscopic mechanism of the metallization of liquid selenium under pressure is studied by *ab initio* molecular dynamics simulations. From the obtained electronic properties, such as the electronic density of states and the bond-overlap population, the pressure-induced metallization is found to be completed at a pressure of approximately 5 GPa, in agreement with recent experimental observations. When the pressure exceeds 5 GPa, the nearest-neighbor distance and the coordination number increase drastically with increasing pressure up to 10 GPa. An important finding is that, during this structural change, there is a microscopic competition between metalliclike and covalentlike interactions, which results in a peculiar atomic structure in this pressure range. The pressure dependence of the self-diffusion coefficient is in qualitative agreement with that of the experimental share viscosity. A comparison with the static structure of liquid tellurium under pressure is also discussed.

DOI: 10.1103/PhysRevB.83.134206 PACS number(s): 61.20.Ja, 71.22.+i, 71.15.Pd

## I. INTRODUCTION

Crystalline selenium and crystalline tellurium under ambient conditions both have a trigonal structure in which each atom is coordinated to two other atoms with strong covalent bonds to form a chain structure. The structural and bonding properties of these crystals are determined by four valence $p$ electrons.[1] Two of these form $\sigma$-type covalent bonds between atoms, and the rest occupy nonbonding states called lone-pair (LP) states. These crystals behave as semiconductors with valence and conduction bands formed by the LP and antibonding $\sigma^*$ states, respectively. Under pressure, a similar sequence of structural transitions is exhibited by crystalline selenium,[2,3] tellurium,[4–7] and their mixtures,[8] along with a discontinuous increase in the coordination number. All of the high-pressure states exhibit metallic properties.

On melting at ambient pressure, the chain structure is basically preserved in liquid Se and Te. While liquid Te exhibits semimetallic properties due to a strong interchain correlation,[9] liquid Se exhibits semiconducting properties, as does the crystalline phase. Since large chain molecules are maintained in liquid Se, it has a high viscosity near the triple point.[10] Accompanying the decrease of the average chain length with increasing temperature and pressure, the electrical conductivity of liquid Se increases, and a metallic state appears near the critical point despite the volume expansion.[11–13] In relation to such semiconductor-metal (SC-M) transitions, the temperature dependence of structure has been thoroughly studied by x-ray diffraction measurements[14] and first-principles theory.[15,16]

It was known from conductivity measurements that the temperature of the SC-M transitions decreases with increasing pressure.[17,18] Recently, Brazhkin *et al.*[19] measured the viscosity of liquid Se at pressures up to 6.3 GPa using real-time radiography. They found that the viscosity decreases considerably with increasing pressure along the melting curve in the semiconducting state, and then experiences a significant drop at the pressure at which metallization occurs. They suggested that this observed viscosity decrease is related to chain defragmentation. However, the detailed pressure effects on the chain structure of liquid Se remain unknown, because x-ray diffraction experiments[20–22] have only been carried out in a limited pressure range. Raty *et al.*[20] investigated a pressure-induced structural change between 3.0 and 4.1 GPa, Tsuji[21] reported x-ray diffraction patterns at 4.4 and 8.4 GPa, and Katayama *et al.*[22] performed x-ray diffraction experiments in the pressure range from 2.6 to 4.9 GPa. These experimental studies suggest that the local atomic structure of metallic liquid Se under pressure is similar to that of liquid Te.

The pressure dependence of the atomic structure of liquid Te has, on the other hand, been investigated in detail, both experimentally and theoretically. Funamori and Tsuji[23] have measured synchrotron x-ray diffraction of liquid Te under pressures of up to 22 GPa. They observed a maximum at about 6 GPa in the pressure versus nearest-neighbor distance curve, while the coordination number increases monotonically with increasing pressure. Shimojo *et al.*[24] have performed *ab initio* molecular dynamics (MD) simulations of liquid Te under pressure. They concluded that there are two stages in the compression process. In the first stage, the nearest-neighbor distance increases with increasing pressure up to 6 GPa, due to the formation of a weak covalent bonding state between Te atoms. In the second stage, the anisotropy of the atomic configuration around each atom decreases with increasing pressure.

In this paper, we investigate the structural, bonding, and dynamic properties of liquid Se under pressure using *ab initio* MD simulations. The purposes of our study are to clarify the structure of liquid Se at high pressures, and to elucidate the microscopic relationship between structural changes and the pressure-induced SC-M transition. Finally, we compare the pressure dependence of the structure of liquid Se to that of liquid Te.

## II. METHOD OF CALCULATION

In the MD simulations, the atomic forces are obtained from the electronic states calculated using the projector-augmented-wave (PAW) method[25,26] within the framework of density functional theory (DFT). The generalized gradient approximation (GGA)[27] is used for the exchange-correlation energy. The plane-wave cutoff energies are 15 and 100 Ry for the electronic pseudo-wave-functions and the

 

TABLE I. Densities $\rho$ (g/cm$^3$) used in MD simulations of liquid Se in the canonical ensemble. The relative volumes $V/V_0$, where $V_0$ is the volume at $\rho = 3.79$ g/cm$^3$ ($P = 0$ GPa, $T = 560$ K), and the time-averaged pressures[34,35] $P$ (GPa) are also listed.

| $\rho$ (g/cm$^3$) | $V/V_0$ | $P$ (GPa) | $T$ (K) |
|---|---|---|---|
| 3.91 | 0.97 | 0.1 | 560 |
| 4.51 | 0.84 | 0.9 | 650 |
| 5.06 | 0.75 | 3.3 | 800 |
| 5.42 | 0.70 | 5.0 | 1000 |
| 5.78 | 0.66 | 7.0 | 1000 |
| 6.14 | 0.62 | 9.4 | 1000 |
| 7.30 | 0.52 | 28.1 | 2000 |
| 7.89 | 0.48 | 39.2 | 2000 |
| 9.52 | 0.40 | 85.9 | 2000 |

pseudo-charge-density, respectively. The energy functional is minimized using an iterative scheme.[28,29] Projector functions are generated for the $4s$, $4p$, and $4d$ states. The $\Gamma$ point is used for Brillouin-zone sampling. The equations of motion for atoms are solved via an explicit reversible integrator[30] with a time step of $\Delta t = 2.4$ fs. A system of 81 atoms in a cubic supercell is used under periodic boundary conditions. The system-size dependence of the atomic structure is discussed in the Appendix.

To determine the density of the liquid state under pressure, a constant-pressure MD simulation[31] is performed for 2.4 ps at each given pressure. The temperatures are chosen to follow the experimental melting curve.[19] Using the time-averaged density, the static and diffusion properties are investigated by MD simulations in the canonical ensemble.[32,33] The time-averaged pressure[34,35] is calculated at each density, and we obtain the results listed in Table I. The thermodynamic states investigated in this study cover a density range from 3.91 to 9.52 g/cm$^3$ and a pressure range from 0.1 to 85.9 GPa. The quantities of interest are obtained by averaging over 14.4–21.6 ps to achieve good statistics after the initial equilibration, which takes at least 2.4 ps.

## III. RESULTS AND DISCUSSION

### A. Structure factor

Figure 1 shows the pressure dependence of the structure factor $S(k)$ of liquid Se. The solid lines represent the calculated $S(k)$, and the results of x-ray diffraction experiments[14,22] are indicated by open circles. The calculated results are in good agreement with experiments. With increasing pressure, the first peak around 1.8 Å$^{-1}$ at 0.1 GPa shifts to larger $k$, and its intensity increases. In contrast, the second peak decreases in height with increasing pressure, and almost disappears above 9 GPa.

### B. Pair distribution function

The pressure dependence of the pair distribution function $g(r)$ of liquid Se is shown by solid lines in Fig. 2. At 0.1 GPa, a sharp first peak is observed at approximately 2.4 Å, and is well separated from the second peak. The first peak reflects the strong covalent bonding between intrachain nearest-neighbor atoms. With increasing pressure, the second peak shifts to

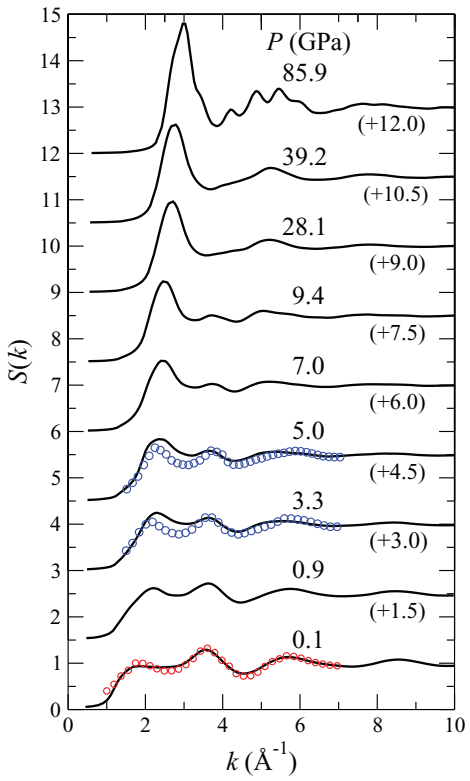


FIG. 1. (Color online) Pressure dependence of the structure factor $S(k)$. The solid lines and open circles represent calculated and experimental[14,22] $S(k)$, respectively. The curves are shifted vertically as indicated by the figures in parentheses.

smaller $r$, and the first minimum becomes shallower. At 7.0 and 9.4 GPa, the minimum almost disappears, and the second peak becomes a shoulder. At higher pressures, the second peak merges into the first, and the peak height increases with increasing pressure.

Figure 3 shows the pressure dependence of the coordination number $N$ and the nearest-neighbor distance $r_1$ [the first-peak position of $g(r)$]. The coordination number is obtained in three ways: (A) $N_A$ is obtained by integrating $4\pi r^2 \rho_0 g(r)$ up to $r_1$, and multiplying it by 2, where $\rho_0$ denotes the number density, (B) $N_B$ is obtained by integrating $4\pi r^2 \rho_0 g(r)$ up to the first-peak position of $4\pi r^2 g(r)$, and multiplying it by 2, and (C) $N_C$ is obtained by integrating $4\pi r^2 \rho_0 g(r)$ up to the first-minimum position of $g(r)$, $r_{min} = 2.7$ Å, at 0.1 GPa. In Fig. 3(a), the circles, squares, and triangles show $N_A$, $N_B$, and $N_C$, respectively. All $N_A$, $N_B$, and $N_C$ decrease slightly with increasing pressure below 5 GPa. Since $g(r)$ has the sharp first peak, the $N_A$ and $N_B$ values are similar. However, above 5.0 GPa, there is a large difference between $N_A$ and $N_B$. While $N_A$ increases almost linearly with the volume reduction above 5 GPa, $N_B$ increases drastically from about 2 to 7 between 5 and 10 GPa. In this pressure range, $g(r)$ has a very broad profile, and, therefore, a discrepancy exists between $N_A$ and $N_B$. Unlike $N_A$ and $N_B$, $N_C$ increases more gradually with pressure. As shown in Fig. 3(b), $r_1$ increases only slightly below 5 GPa. When the pressure exceeds 5 GPa, $r_1$ increases abruptly, reflecting the broad shape of $g(r)$. $r_1$ has a maximum around 20 GPa, and decreases with decreasing volume above

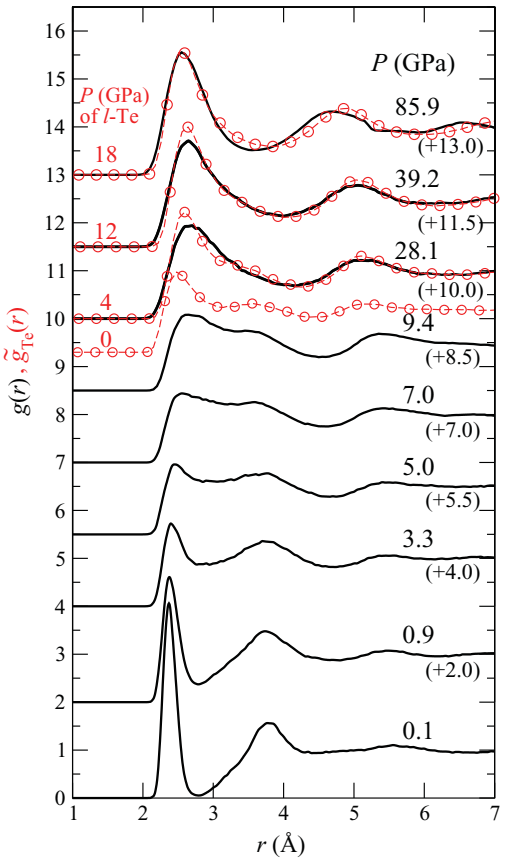


FIG. 2. (Color online) Pressure dependence of the pair distribution function $g(r)$. The solid lines show $g(r)$ for liquid Se obtained here. The dashed lines with open circles show a modified pair distribution function $\tilde{g}_{\mathrm{Te}}(r)$ for liquid Te obtained from previous *ab initio* MD simulations.[24] See the text for details of $\tilde{g}_{\mathrm{Te}}(r)$.

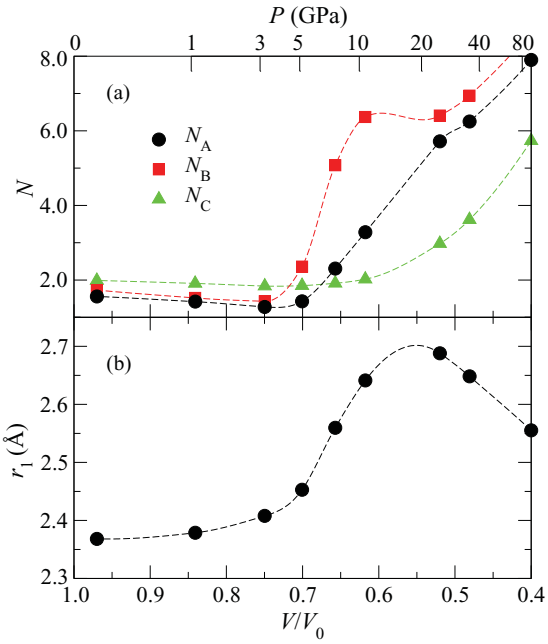


FIG. 3. (Color online) (a) Pressure dependence of the average coordination number $N$. The circles, squares, and triangles indicate $N_{\mathrm{A}}$, $N_{\mathrm{B}}$, and $N_{\mathrm{C}}$, respectively, as calculated by three different definitions (see text). (b) Pressure dependence of the nearest-neighbor distance $r_1$.

that pressure. A more detailed discussion of the changes in the local structure will be given in Sec. III F.

### C. Electronic density of states

Figure 4 shows the pressure dependence of the total electronic density of states (DOS), $D(E)$, and the angular-momentum $l$-dependent partial DOS, $D_l(E)$. $D(E)$ is related to $D_l(E)$ as $D(E) = \sum_l D_l(E)$. In $D(E)$, there are two segments below the Fermi level ($E_F = 0$) at 0.1 GPa. The electronic states below $-10$ eV and above $-6$ eV originate mainly from the $4s$ and $4p$ electrons, respectively. They are well separated even when the pressure is increased. There are two peaks at about $-5$ and $-2$ eV, which correspond to $p$-like bonding and $p$-like nonbonding states, respectively. The DOS above $E_F$ originates from $p$-like antibonding states. At 0.1 GPa, $D(E)$ has a deep dip around $E_F$ corresponding to the semiconducting properties of liquid Se. The value of $D(E_F)$ increases when the pressure is increased to 5.0 GPa. Since $D(E_F)$ does not change significantly above 5.0 GPa, it is concluded that the metallization is completed around this pressure.

Note that the deep dip around $E_F$ at 0.1 GPa becomes shallower at 0.9 GPa, which may indicate that the system starts to have metallic properties. However, liquid Se still behaves as a semiconductor in this pressure region.[17,18] Since the GGA usually underestimates the energy of unoccupied states, the dip in the theoretical $D(E)$ would appear to be too shallow at 0.9 GPa. Nevertheless, we expect that our conclusions will be unchanged, because a correction to the GGA will change the calculated results quantitatively in only small amounts.

### D. Bond-overlap population

We use population analysis[36,37] to clarify the changes in bonding properties due to the SC-M transition. By expanding the electronic wave functions in an atomic-orbital basis set, we obtain the overlap population $O_{ij}(t)$ between the $i$th and $j$th atoms as a function of time $t$. $O_{ij}(t)$ gives a semiquantitative estimate of the strength of the covalentlike bonding between atoms. Figure 5 shows the pressure dependence of the time evolution of $O_{ij}(t)$ associated with an arbitrarily selected ($i$th) atom. We select its surrounding ($j$th) atoms, whose distance from the $i$th atom becomes shorter than 4 Å within 3 ps. At 0.1 GPa, each atom has finite $O_{ij}(t)$ with two neighboring atoms reflecting the chain structure, and the bond exchange scarcely occurs. When the pressure is increased to 0.9 GPa, $O_{ij}(t)$ can be exchanged while the twofold coordination of each atom is mostly maintained. The threefold coordinated defects do not exist stably, because more than two $O_{ij}(t)$ have finite values only temporarily. Above 3.3 GPa, the bond switching occurs more frequently at higher pressures. At 9.4 GPa, $O_{ij}(t)$ do not keep high values $>0.5$, but rise and fall in a range of 0–0.5, which suggests that no stable covalent bonds exist between atoms. A discussion on the bonding properties at 9.4 GPa will be given in Sec. III F.

Figure 6 shows the time-averaged distribution $p(\overline{O})$ of the overlap populations $O_{ij}(t)$. In $p(\overline{O})$, there is a clear peak

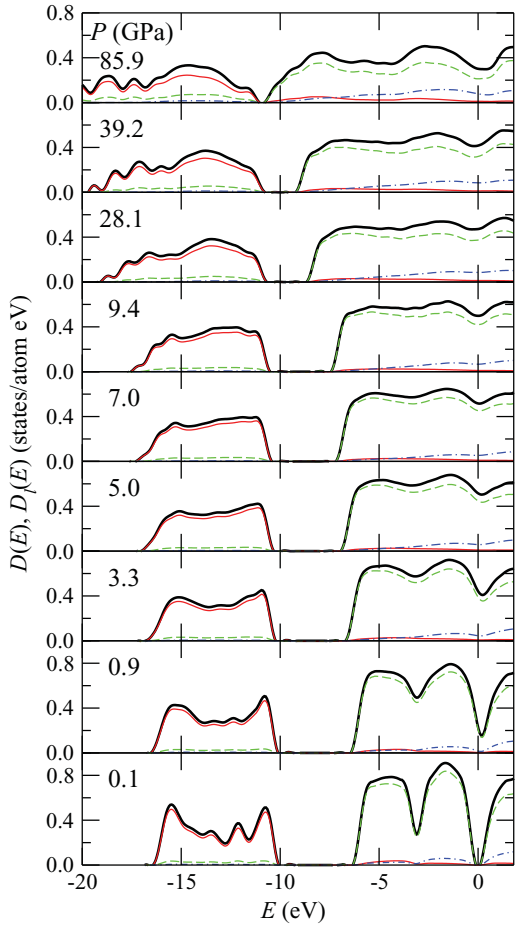


FIG. 4. (Color online) Pressure dependence of the electronic density of states $D(E)$ and the angular-momentum $l$-dependent partial electronic density of states $D_l(E)$. The bold solid lines indicate $D(E)$. The thin solid, dashed, and dot-dashed lines indicate $D_l(E)$ for $l = 0$, 1, and 2, respectively.

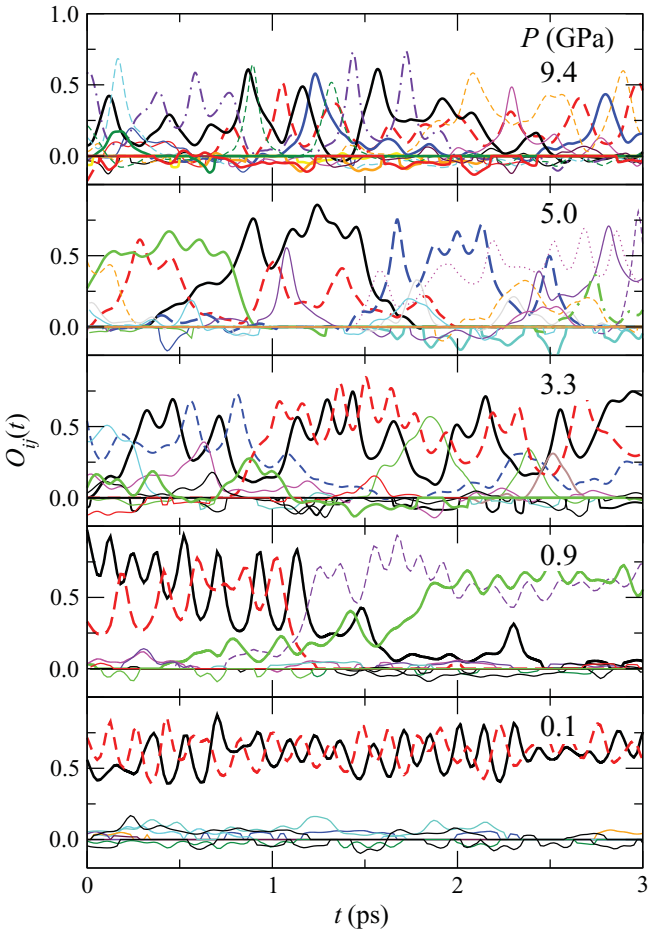


FIG. 5. (Color online) Pressure dependence of the time evolution of the overlap populations $O_{ij}(t)$ associated with an arbitrarily selected ($i$th) atom. The surrounding ($j$th) atoms are selected when the atomic distance from the $i$th atom becomes shorter than 4 Å within 3 ps.

at about $\overline{O} = 0.7$ at 0.1 GPa. With increasing pressure, the peak shifts to smaller $\overline{O}$ and becomes broad, indicating that the covalent-bonding interaction weakens as the metallization occurs. Above 5.0 GPa, the profile of $p(\overline{O})$ for $\overline{O} > 0$ has no clear peak, although there is a recognizable shoulder around $\overline{O} = 0.3$ below 10 GPa. The peak around $\overline{O} = -0.05$ at 0.1 GPa corresponds to the repulsive interaction between next-nearest-neighbor atoms within the chain due to the LP states. This peak becomes broad with increasing pressure, and a new peak grows in the negative $\overline{O}$ region above 10 GPa.

### E. Pressure-induced metallization of liquid Se

As was seen in Fig. 3(a), all $N_A$, $N_B$, and $N_C$ are almost 2 below 5 GPa, indicating that the chain structure remains up to this pressure. The slight decrease of these values with increasing pressure indicates that the average chain length shortens under pressure. These results suggest that liquid Se is metallized under compression while the chain structure is maintained, in a similar manner as metallization near the critical point accompanying volume expansion.[14,15] Note that the first minimum of $g(r)$ becomes shallower with increasing pressure from 0 to 5 GPa (Fig. 2), which is a result of frequent bond breaking and bond formation in Se chains under pressure as shown in Fig. 5. Such strong interactions between Se chains along with their rearrangement play an important role in the pressure-induced metallization.

### F. Covalentlike interaction in the metallic state

Between 5 and 10 GPa, $N_A$, $N_B$, and $r_1$ increase rapidly with compression, as shown in Fig. 3. This indicates a considerable structural change in this pressure range. As shown in Fig. 2, $g(r)$ at 7.0 and 9.4 GPa have a peculiar shape in the sense that $g(r)$ has no clear peaks, and exceeds 1 over a wide range of $r$ from 2.4 to 4.0 Å. This characteristic profile of $g(r)$ suggests that covalent interactions disappear in liquid Se at these pressures. To clarify the origin of the peculiar shape of $g(r)$, it is essential to uncover the inherent structure of these states by eliminating the effects of thermal fluctuations. For this purpose, we decrease the temperature of the system at 9.4 GPa from 1000 to 500 K, while maintaining a fixed volume, i.e., $V/V_0 = 0.62$. Figure 7 compares $g(r)$ obtained at 500 K with that at 1000 K. When the temperature effects are reduced, two peaks appear at 2.6 and 3.7 Å.[38] The coordination numbers at 500 K are $N_A = 3.2$, $N_B = 3.4$, and $N_C = 2.0$. Since $g(r)$

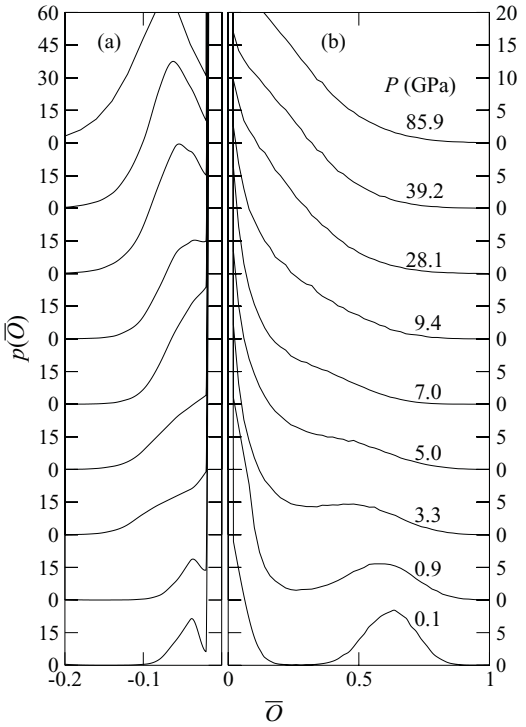


FIG. 6. Pressure dependence of the distribution of the bond-overlap populations $p(\overline{O})$ for (a) $\overline{O} < 0$ and (b) $\overline{O} > 0$.

has a clear first peak, $N_A$ and $N_B$ are consistent with each other in their values. At 1000 K, the dip between these two peaks disappears due to larger thermal motion of the atoms, so that $g(r)$ at 7.0 and 9.4 GPa has a peculiar shape.

To examine the bonding properties between atoms at this volume in detail, the time evolution of $O_{ij}(t)$ at 500 K is shown in Fig. 8(a). The $i$th atom interacts with several atoms with finite $O_{ij}(t) > 0$, out of which are one or two atoms with large $O_{ij}(t) \sim 0.4$. Figure 8(b) shows the time evolution of the distance $d_{ij}(t)$ between the $i$th and $j$th atoms, whose $O_{ij}(t)$ is displayed by the bold line in Fig. 8(a). It is obvious that $O_{ij}(t)$ is strongly correlated with $d_{ij}(t)$; for larger distances $d_{ij}(t) \sim 3.5$ Å for $t < 1.5$ ps, $O_{ij}(t)$ is nearly zero, and for smaller distances $d_{ij}(t) \sim 2.6$ Å after 1.5 ps, $O_{ij}(t)$ becomes finite. At higher temperatures, surrounding atoms move more continually between these two nonbonding and bonding sites

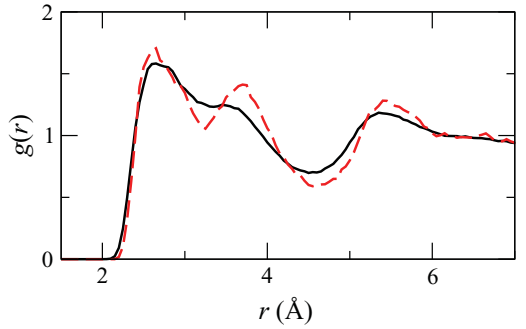


FIG. 7. (Color online) Pair distribution function $g(r)$ at $V/V_0 = 0.62$. The solid and dashed lines represent $g(r)$ at 1000 and 500 K, respectively.

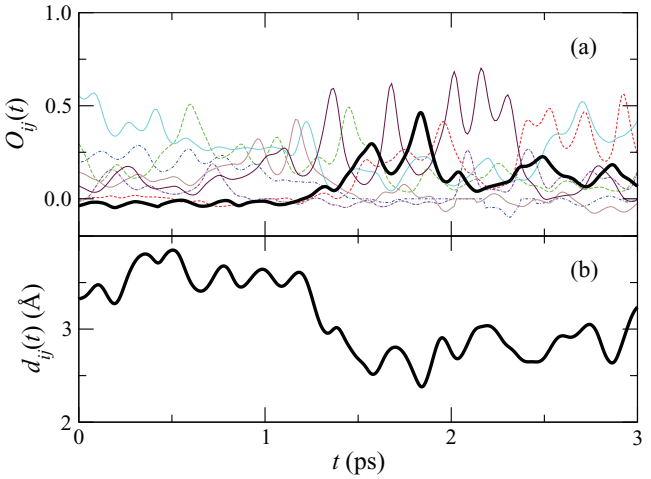


FIG. 8. (Color online) (a) The time evolution of the overlap populations $O_{ij}(t)$ at $V/V_0 = 0.62$ and $T = 500$ K. $O_{ij}(t)$ are plotted associated with an arbitrarily selected ($i$th) atom. The surrounding ($j$th) atoms are selected when the atomic distance from the $i$th atom becomes shorter than 4 Å within 3 ps. (b) The time evolutions of the atomic distance $d_{ij}(t)$ for the atomic pair corresponding to the bold line in (a).

with the central atom as shown in Fig. 5. In conclusion, each atom interacts with neighboring atoms through covalentlike bonding with finite $O_{ij}(t) > 0$ as a remnant of the chain structure, even though the system is in the metallic state in the pressure range from 5 to 10 GPa (the volume $V/V_0$ range from 0.6 to 0.7). These atomic pairs form the first peak of $g(r)$ at 2.6 Å (Fig. 7).

### G. Comparison with liquid Te

According to *ab initio* MD simulations,[24] the coordination number of liquid Te is $N_A = 2.5$, 5.0, 6.3, and 7.0 at 0, 4, 12, and 18 GPa, respectively. Considering this pressure dependence, $g_{Te}(r)$ of liquid Te is compared with $g(r)$ of liquid Se as displayed by the dashed lines with open circles in Fig. 2. For this comparison, $\tilde{g}_{Te}(r) \equiv g_{Te}(\alpha r)$ is plotted, where $\alpha = R_1/r_1$ with $R_1$ and $r_1$ being the first-peak positions of $g_{Te}(r)$ and $g(r)$, respectively, so that $\tilde{g}_{Te}(r)$ and $g(r)$ have the first peaks at the same position. Although there is no state in liquid Se corresponding well to that of liquid Te at 0 GPa, the shape of $\tilde{g}_{Te}(r)$ for liquid Te under pressure is in good agreement with that of liquid Se above 28.1 GPa. These results confirm that the local structure of liquid Se at high pressures is similar to that of liquid Te.

### H. Dynamic properties

Figure 9(a) shows the diffusion coefficients $D$ as a function of pressure, estimated from the slopes of the mean-squared displacement as

$$D = \lim_{t\to\infty} \frac{\langle \{\boldsymbol{r}_i(t) - \boldsymbol{r}_i(0)\}^2 \rangle}{6t}, \quad (1)$$

where $r_i(t)$ is the position of the $i$th atom at time $t$, and $\langle \cdots \rangle$ indicates an average over all atoms and time. We see that $D$ of liquid Se increases with increasing pressure up to about 5 GPa and temperature up to 1000 K along the

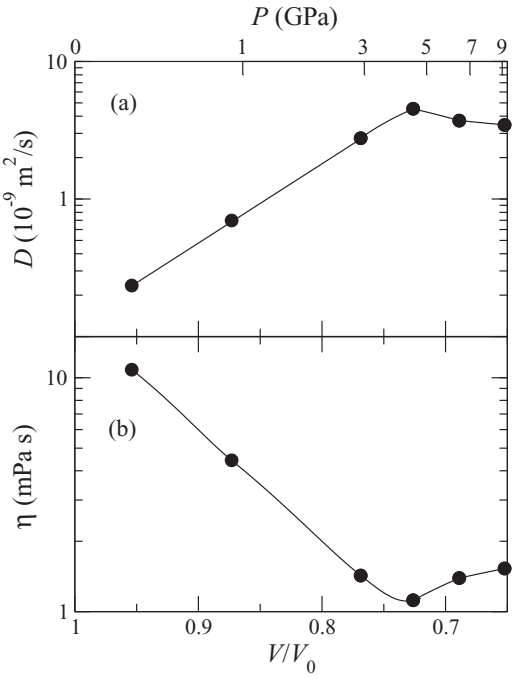


FIG. 9. Pressure dependence of (a) the diffusion coefficient $D$ and (b) the share viscosity $\eta$.

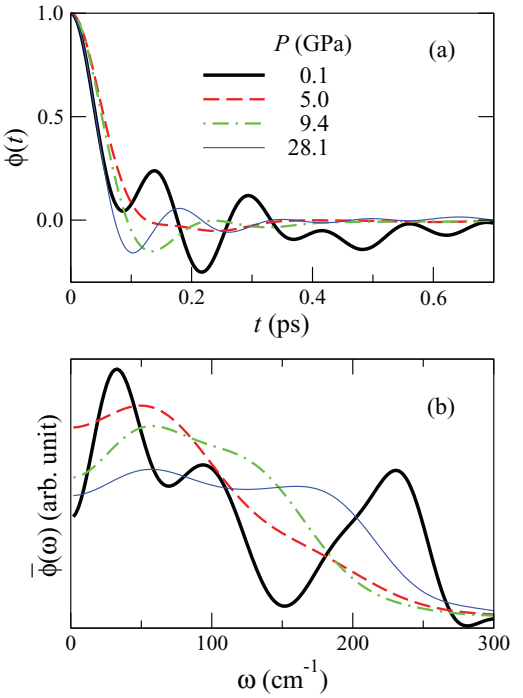


FIG. 10. (Color online) Pressure dependence of (a) the normalized velocity autocorrelation function $\phi(t)$ and (b) its Fourier transform $\overline{\phi}(\omega)$.

experimental melting curve. Since this pressure dependence of $D$ results from changes in both temperature and pressure, we will not discuss the pure effect of pressure on the dynamic properties. It should be noted, however, that the volume contraction enhances atomic diffusion in covalent liquids, such as liquid $SiO_2$ (Ref. 39) and $B_2O_3$,[40] due to weakening of the strong covalent-bonding interaction between atoms. In liquid Se, the same pressure effect should exist well below 5 GPa, at which the liquid has semiconducting properties. The pressure dependence of the viscosity $\eta$ is estimated using the Stokes-Einstein formula as shown in Fig. 9(b), which is in qualitative agreement with the experimental results.[19,41]

The normalized velocity autocorrelation function $\phi(t)$ and its Fourier transform $\overline{\phi}(\omega)$ are defined as

$$\phi(t) = \frac{\langle \boldsymbol{v}_i(t) \cdot \boldsymbol{v}_i(0) \rangle}{\langle \boldsymbol{v}_i(0) \cdot \boldsymbol{v}_i(0) \rangle}, \tag{2}$$

$$\overline{\phi}(\omega) = \int_0^\infty \phi(t) \cos(\omega t)\, dt, \tag{3}$$

where $\boldsymbol{v}_i(t)$ is the velocity of the $i$th atom at time $t$. Figure 10 shows the pressure dependence of $\phi(t)$ and $\overline{\phi}(\omega)$. At 0.1 GPa, $\phi(t)$ exhibits an oscillating behavior, reflecting strong covalent bonding in the semiconducting state. The peak of $\overline{\phi}(\omega)$ at 230 $cm^{-1}$ corresponds to the stretching motion of Se-Se bonds. Since the covalentlike interaction becomes weak with increasing pressure as shown in Fig. 6, $\phi(t)$ exhibits weaker oscillations as displayed by the dashed line for 5 GPa, and the corresponding $\overline{\phi}(\omega)$ consists of a broad peak at a lower frequency $\sim$50 $cm^{-1}$. On the other hand, in the metallic state, $\phi(t)$ again shows oscillation as seen at 9.4 and 28.1 GPa, probably due to cage effects similar to those exhibited by typical liquid metals. $\overline{\phi}(\omega)$ has a shoulder or broad peak at a relatively high frequency around 150 $cm^{-1}$.

## IV. SUMMARY

We have investigated the structural and bonding properties of liquid Se under pressures of up to 85.9 GPa using *ab initio* molecular dynamics simulations. Analysis of the pair distribution function, the electronic density of states, and the bond-overlap population revealed the microscopic mechanism of the pressure-induced metallization of liquid Se. A covalentlike interaction exists in the metallic state at pressures ranging from 5 to 10 GPa, which results in a peculiar shape of the pair distribution function. The present work confirms that the local structures of liquid Se and Te under high pressure are similar. The pressure dependence of

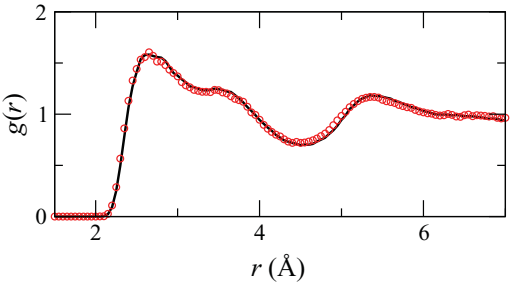


FIG. 11. (Color online) Pair distribution functions $g(r)$ at $V/V_0 = 0.62$. The solid line and circles represent $g(r)$ obtained for the 81- and 160-atom systems, respectively.

the dynamic properties, such as the diffusion coefficient and the velocity autocorrelation function, was also discussed.

## ACKNOWLEDGMENTS

The present work was supported by a Grant-in-Aid for JSPS Fellows, and by Hamamatsu Photonics K.K., Japan. The authors thank the Research Institute for Information Technology, Kyushu University for the use of facilities. The computations were also carried out using the computer facilities at the Supercomputer Center, Institute for Solid State Physics, University of Tokyo.

## APPENDIX: SIZE DEPENDENCE OF STRUCTURE

In this appendix, we report the system size dependence of the structure of liquid Se. For a system of 160 Se atoms, two times larger than the system discussed in the text, an *ab initio* MD simulation is carried out at a temperature of 1000 K. The volume is determined by doubling the system size of 81 atoms at $V/V_0 = 0.62$. A comparison of $g(r)$ is shown in Fig. 11. The two $g(r)$ are almost identical, which suggests that the 81-atom system is sufficiently large to investigate the pressure dependence of the structure of liquid Se.

[1] W. A. Harrison, *Electronic Structure and the Properties of Solids* (Freeman, San Francisco, 1980).
[2] Y. Akahama, M. Kobayashi, and H. Kawamura, Phys. Rev. B **47**, 20 (1993).
[3] M. I. McMahon, C. Hejny, J. S. Loveday, L. F. Lundegaard, and M. Hanfland, Phys. Rev. B **70**, 054101 (2004).
[4] J. C. Jamieson and D. B. McWhan, J. Chem. Phys. **43**, 1149 (1965).
[5] K. Aoki, O. Shimomura, and S. Minomura, J. Phys. Soc. Jpn. **48**, 551 (1980).
[6] P. Vulliet and J. P. Sanchez, Phys. Rev. B **58**, 171 (1998).
[7] G. Parthasarathy and W. B. Holzapfel, Phys. Rev. B **37**, 8499 (1988).
[8] Y. Ohmasa, I. Yamamoto, Y. A. O. Makoto, and H. Endo, J. Phys. Soc. Jpn. **64**, 4766 (1995).
[9] T. Tsuzuki, M. Yao, and H. Endo, J. Phys. Soc. Jpn. **64**, 485 (1995).
[10] J. C. Perron, J. Rabit, and J. F. Rialland, Philos. Mag. B **46**, 321 (1982).
[11] H. Hoshino, R. W. Schmutzler, W. W. Warren, and F. Hensel, Philos. Mag. **33**, 255 (1976).
[12] W. W. Warren Jr. and R. Dupree, Phys. Rev. B **22**, 2257 (1980).
[13] H. Ikemoto, I. Yamamoto, M. Yao, and H. Endo, J. Phys. Soc. Jpn. **63**, 1611 (1994).
[14] K. Tamura and M. Inui, J. Phys. Condens. Matter **13**, R337 (2001).
[15] F. Shimojo, K. Hoshino, M. Watabe, and Y. Zempo, J. Phys. Condens. Matter **10**, 1199 (1998).
[16] F. Kirchhoff, G. Kresse, and M. J. Gillan, Phys. Rev. B **57**, 10482 (1998).
[17] V. V. Brazhkin, S. V. Popova, and R. N. Voloshin, Phys. Lett. A **166**, 383 (1992).
[18] V. V. Brazhkin and A. G. Lyapin, J. Phys. Condens. Matter **15**, 6059 (2003).
[19] V. V. Brazhkin, K. Funakoshi, M. Kanzaki, and Y. Katayama, Phys. Rev. Lett. **99**, 245901 (2007).
[20] J. Y. Raty, J. P. Gaspard, T. Le Bihan, M. Mezouar, and M. Bionducci, J. Phys. Condens. Matter **11**, 10243 (1999).
[21] K. Tsuji, J. Non-Cryst. Solids **117–118**, 27 (1990).
[22] Y. Katayama, T. Mizutani, W. Utsumi, O. Shimomura, and K. Tsuji, Phys. Status Solidi B **223**, 401 (2001).
[23] N. Funamori and K. Tsuji, Phys. Rev. B **65**, 014105 (2001).
[24] F. Shimojo, K. Hoshino, and Y. Zempo, J. Phys. Soc. Jpn. **72**, 2822 (2003).
[25] P. E. Blöchl, Phys. Rev. B **50**, 17953 (1994).
[26] G. Kresse and D. Joubert, Phys. Rev. B **59**, 1758 (1999).
[27] J. P. Perdew, K. Burke, and M. Ernzerhof, Phys. Rev. Lett. **77**, 3865 (1996).
[28] G. Kresse and J. Hafner, Phys. Rev. B **49**, 14251 (1994).
[29] F. Shimojo, R. K. Kalia, A. Nakano, and P. Vashishta, Comput. Phys. Commun. **140**, 303 (2001).
[30] M. Tuckerman, B. J. Berne, and G. J. Martyna, J. Chem. Phys. **97**, 1990 (1992).
[31] G. J. Martyna, D. J. Tobias, and M. L. Klein, J. Chem. Phys. **101**, 4177 (1994).
[32] S. Nosé, Mol. Phys. **52**, 255 (1984).
[33] W. G. Hoover, Phys. Rev. A **31**, 1695 (1985).
[34] O. H. Nielsen and R. M. Martin, Phys. Rev. B **32**, 3780 (1985).
[35] A. Dal Corso and R. Resta, Phys. Rev. B **50**, 4327 (1994).
[36] R. S. Mulliken, J. Chem. Phys. **23**, 1841 (1955).
[37] F. Shimojo, A. Nakano, R. K. Kalia, and P. Vashishta, Phys. Rev. E **77**, 066103 (2008).
[38] When the system of $V/V_0 = 0.62$ is further quenched to nearly 0 K, the first peak at 2.6 Å is split into two peaks at 2.6 and 2.9 Å. Note that no such peak split is observed by quenching the system of $V/V_0 \leqslant 0.52$.
[39] B. B. Karki, D. Bhattarai, and L. Stixrude, Phys. Rev. B **76**, 104205 (2007).
[40] S. Ohmura and F. Shimojo, Phys. Rev. B **80**, 020202 (2009).
[41] D. E. Harrison, J. Chem. Phys. **41**, 844 (1964).